MAP MAKING WITH REMOTE SENSING DATA*

THIERRY TOUTIN
Canada Centre for Remote Sensing
588 Booth Street,
Ottawa, Ontario, Canada, K1A 0Y7

Abstract

Map making with remote sensing data requires geometric and radiometric processing methods (monoscopic and stereoscopic) adapted to the nature and characteristics of the data in order to extract the best cartographic and topographic information. For the monoscopic method, different geometric and radiometric processing techniques are compared and evaluated, quantitatively and qualitatively with their impact on the resulting composite images, using panchromatic SPOT and airborne SAR images. The techniques that take into account the nature of the data give better results, with greater integrity: a subpixel geometric accuracy with high-quality composite images, which are sharp and precise and containing well-defined cartographic elements and data that are easy to interpret and closer to physical reality. The stereoscopic method still is the most common method used by the mapping, photogrammetry and remote sensing communities to extract three-dimensional information. It is successfully applied either to images in the visible spectrum or radar images to generate digital elevation model with an accuracy of tens of metres depending of the data source.

1. Introduction

Throughout history, humans have tried to represent what they saw and understood through images. Everything from cave walls, to canvases, to computer screens have been used to express perception of our surroundings. Maps have been one way to show the relationship between humans and their environment. Towns, roads, rivers, mountains, valleys, and where the land meets the sea, have been drawn in an organized

* In Proceedings of the NATO Advanced Research Workshop on Remote Sensing for Environmental Data in Albania: A Strategy for Integrated Management, 6-10 October 1999, Tirana, Albania, pp. 65-87.

fashion for centuries. Mapmakers have always sought ways in which to represent both the location and the three dimensional shape of land.

Not so long ago, a hill top view was the largest vista from which to observe nature's workings. Discoveries in optics, photography and flight have allowed us to see the Earth as never before. Advanced methods in computing and signal processing technologies have enabled us to increase our ability to visualize and perceive the Earth's surface. Today, Earth observation satellites orbit our planet collecting data needed to produce images which allow us to monitor, understand and plan the use of our world's resources. However, specific processing methods have to be performed on the satellite images to extract information before making maps.
Two conventional methods can be considered to extract information from remote sensing data (Figure 1):

1. The monoscopic method which uses one image and an existing digital elevation model (DEM) to generate an ortho-image from which only planimetric features with their 2-D map coordinates (XY) can be extracted; and
2. the stereoscopic method which uses two images to generate a "virtual" stereo-model from which planimetric and altimetric features with their 3-D map coordinates (XY and/or Z) can be extracted

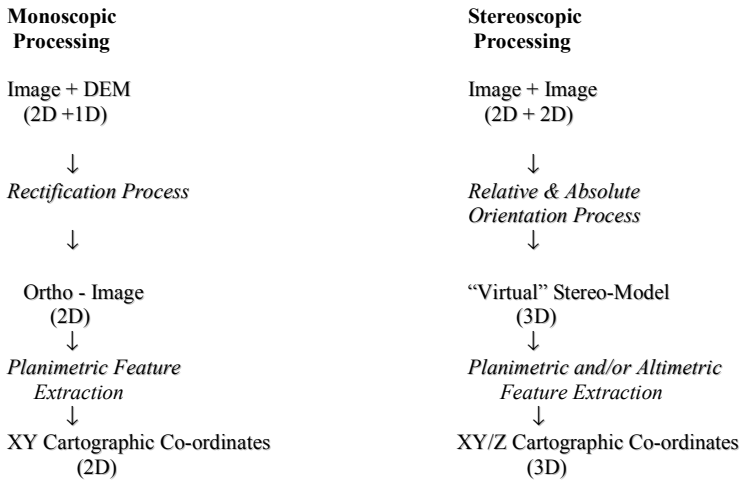

Figure 1. Description of the monoscopic and stereoscopic processing methods for 2D or 3D cartographic feature extraction.

In the first method, the DEM has to be produced from any method (contour lines digitizing, stereoscopy, interferometry, etc.) with some errors. These errors will propagate through the rectification process and the planimetric features extraction. Furthermore, resampling during the rectification process degrades not only the image geometry and radiometry, but also the image interpretability.

In the second method, the brain can generate the perception of depth with two images from same or different sensors. The stereoscopic fusion of multi-sensor images then provides a virtual three-dimensional model of the terrain surface, and the stereo plotting enables the extraction of cartographic features directly in the map reference system. Conversely to the first method, the planimetric accuracy of feature positioning is not affected by any elevation error. Furthermore, since the stereo-extraction is done directly on the raw images, no re-sampling degrades the image radiometry, geometry and interpretability.

The main objective of this paper is to present the basic processing steps of these two conventional methods, which are necessary to generate maps from remote sensing data. Comparisons and performances of different techniques, tools and softwares for the processing steps are presented. Finally, some examples and results of map making with different satellite images from these two methods are showed.

2. Monoscopic Processing

The monoscopic processing of satellite images can be based on the concept of "geocoded images", to define value-added products [1]. Photogrammetrists, however, prefer the term "ortho-image" in referring to a unit of geocoded data. To integrate different satellite images under this concept, each raw image must be separately converted to an ortho-image so that each component ortho-image of the data set is registered pixel by pixel and the different radiometries can then be combined [2].

The composite images are products resulting from the integration of different images. Their creation requires two distinct processing steps to ensure that those elements, which are spatially and spectrally separable in the original images, are also separable in the composite images:

- geometric processing to ensure that each pixel in the ortho-images corresponds to the same ground element;
- radiometric processing to merge the information from each image in a common image, such that the best spectral information from each image is preserved.

There are many references in the literature, which combine and/or compare the data in the visible and microwave spectra. Early works by [3, 4, 5, 6] and many others dealt mainly with the integration of Landsat and Seasat data, although other geocoded data were also used [7].

The technique most commonly used is image-to-image registration with a previously geocoded reference image. This registration uses polynomial or spline functions with many tie points between the images. However, these authors generally report the difficulty of finding such tie points between the images, because they are imaged differently by sensors, which have highly variable geometries and responses to

illumination. Errors resulting from this method are of a few pixels, which then generate errors in the radiometric merging of the various ortho-images. The effect is even more significant in mountainous terrain. It is not the best appropriate technique to generate maps.

Consequently, to demonstrate the interest of geometric and radiometric processing techniques suited to the nature and characteristics of the different images, and to measure the impact of the processing tools, it is a requisite:

- to compare different geometric and radiometric processing tools; and
- to quantitatively and qualitatively evaluate the impact of different processing tools on the resulting composite image.

Two techniques of geometric correction are compared: the polynomial functions generally used and a rigorous photogrammetric method developed at the Canada Centre for Remote Sensing (CCRS) [8]. The latter technique allows the integration of DEM into the correction for a better accuracy. Four techniques of merging the radiometric information from the resulting ortho-images are evaluated: red-green-blue, principal components, intensity-hue-saturation and high-pass filter. To enable the evaluation of the two geometric correction techniques significant and to be extrapolated, different images (VIR and SAR; spaceborne and airborne) are used:

- a SPOT-P raw image (level 1A) acquired June 20th, 1987 at a highly tilted viewing angle (+29.3°) and the ephemeris and attitude data related to this image;
- four airborne synthetic aperture radar (SAR) images (north-south flight direction) acquired September 11th, 1990 by the CCRS radar (C-HH, narrow mode, angle of 45° to 76°, ground distance, 4096 pixels by 10,000 lines, pixel spacing of 4.0 by 4.31 m) [9].

Since the width of a SAR image swath is approximately 16 km, two adjacent images were taken pointing east and two others pointing west to create two radiometrically different SAR mosaics over the test area (26 by 40 km). The SPOT-P image has a grey-scale dynamic range of 17 to 60. No radiometric processing was done, except linear stretching on 8 bits. The SAR images were processed in real time in the aircraft and were encoded on 8 bits. No radiometric processing was done of these images.

2.1. GEOMETRIC PROCESSING

While it is known that polynomial functions are not suitable for accurately correcting airborne or space images, many users still apply them, without knowing the implications for subsequent processing operations and the resulting products. The purpose of this comparison is primarily to evaluate and show the impact of these various processing techniques on the results and the composite image.

For both methods (polynomial and photogrammetric), the processing steps are more or less similar, except for the viewing parameters and the altimetry (ground control points and DEM) involved in the photogrammetric method:

- acquisition of parameters of the viewing geometry (for the photogrammetric method only);
- acquisition of ground control points (GCPs): image coordinates and ground coordinates X, Y, (Z);
- calculation of parameters of the polynomial or photogrammetric model;
- cubic-convolution resampling (with DEM) to create the ortho-images and mosaics, with the same pixel size; and
- registration of the vector file to check the results.

Since the polynomial methods, with their formulation, are well known and documented in [10], only few characteristics are given. The polynomial function of the 1^{st} degree allows the correction of translation, rotation, scaling in both axes and obliquity. Polynomial functions of a higher degree (mainly 2^{nd} and 3^{rd}) enable us to correct larger distortions. However, they are generally limited (small image, flat relief and so on), as they do not reflect the causes of distortions during formation of the image. Moreover, one of the assumptions of these functions is that the ground is flat (with no curvature of the Earth), and without relief.

The photogrammetric model, with its formulation, has been described in detail for different images [8]. This parametric model represents the physical law of transformation from ground space to image space. The development of the final equations is based on principles related to photogrammetry (collinearity condition), orbitography (flight path represented by an osculatory ellipse), geodesy (use of a reference ellipsoid) and cartography (conformity of the projection). It allows integration and combination of the different distortions during image formation, as follows:

- distortions related to the platform (position, velocity, orientation);
- distortions related to the sensor (orientation angles, line integration time, instantaneous field of view);
- distortions related to the Earth (geoid-ellipsoid), including relief; and
- distortions related to the map projection (ellipsoid-map plane).

The main characteristics and comparison of the two processing methods (polynomial and photogrammetric) are summarized in Table 1.

2.2. RADIOMETRIC PROCESSING

There are a number of methods for merging spectral information from different images [11]:

- red-green-blue coding (RGB);

- principal component analysis (PCA);
- intensity-hue-saturation coding (IHS); and
- high-pass filter (HPF).

TABLE 1. Comparison of characteristics for polynomial and photogrammetic methods

POLYNOMIAL METHOD	PHOTOGRAMMETRIC METHOD
Does not respect the viewing geometry	Respects the viewing geometry
Not related to distortions	Reflects the distortions
Does not introduce attitude data	Uses ephemeris and attitude data
Does not use DEM	Uses DEM or near elevation
Corrects image locally at the GCPs	Corrects the image globally
Does not filter blunders	Filters blunders with the knowledge of the geometry
Individual adjustments of one image	Simultaneous adjustment of more than one image
Image-to-image correction	Image-to-ground correction
Needs many (>20) GCPs	Need few (3-8) GCPs
Sensitive to GCPs distribution	Not sensitive to GCPs distribution
Problem of choice for tie points	GCPs choice as a function of each image

RGB coding is used directly with three images, assigning each ortho-image to a colour: such as SPOT-P in red, SAR-west in green and SAR-east in blue.

The PC method is a statistical method, which transforms by linear combination a data set of variables correlated among themselves into new decorrelated variables. This method generates new orthogonal axes in radiometric space called principal components. The sum of the variance remains unchanged and each consecutive PC has a decreasing level of variance. Depending on the number of images available, the first three PCs are used or one of the PCs can be replaced by another image. In the case of three images, the three resulting PCs of the PCA are used.

IHS coding can be used in two ways:

- the images are used directly to modulate the RGB display of the IHS coding; some authors use the image with the higher spatial resolution, or the SAR, for intensity [12], while others advise modulating saturation rather than intensity [13]; and
- the IHS parameters are calculated on the basis of three images or spectral bands, then one of the parameters is replaced by a fourth image (of higher resolution, or a SAR) and the RGB reverse transformation is performed to merge the images.

Since only three ortho-images are available in our experiment, only the first method of IHS coding is used in the comparisons of the various radiometric merges.

In the HPF method, we use a high-pass filter to process the image with the highest spatial resolution and then combine it, pixel by pixel, with the image having the lowest spatial resolution but the highest spectral resolution. Thus this method combines the spatial information from the image of higher spatial resolution with the spectral information from the image of higher spectral resolution. It applies mainly to combining a panchromatic SPOT-P or SAR image with multiband Landsat-TM or SPOT-XS image. This tool does not apply in our experiment because the images (SPOT-P and airborne SAR) have approximately the same spatial resolution.

2.3. ANALYSIS OF THE RESULTS

2.3.1. *Geometric Processing*

Analysis of the geometric processing results is done in two stages:

- quantitative analysis involving the residuals on the GCPs, the errors on the independent check points (ICPs) and comparison with the vector file;
- qualitative analysis involving a comparison of the cartographic elements (roads, rivers, forest, cutovers and so on) on the two ortho-images.

Table 2, based on 15 GCPs, gives the root-mean-square (RMS) and maximum residuals (in metres) of the calculation of geometric correction models for the photogrammetric method and the polynomial methods (2^{nd} and 3^{rd} orders). Although in the photogrammetric method only four ground control points for SPOT-P and seven for SAR are necessary and the photogrammetric model is not sensitive to the number of GCPs [8], 15 GCPs were used for consistency in the comparison of results between the two techniques.

TABLE 2. Root mean square and maximum residuals (metres) on 15 GCPs for the monoscopic processing.

	IMAGE	SPOT-P		SAR1-EST		SAR2-EST		SAR1-EAST		SAR2-EAST		ALL	
METHOD	Residuals	Rx	Ry	Rx	Ry	Rx	Ry	Rx	Ry	Rx	Ry	Rx	Ry
Photogram-	RMSR	2.7	3.1	1.0	2.5	6.3	4.9	6.1	6.1	2.9	4.3	3.5	3.6
metric	Rmax	-5.0	7.6	- 1.7	4.4	-10.2	-9.9	10.0	10.6	6.4	10.6	7.8	-7.3
Polynomial	RMSR	23.1	3.4	4.9	3.7	13.8	4.4	14.0	6.3	13.2	5.1	-	-
2^{nd} order	Rmax	-50.3	6.0	-10.8	7.4	-20.8	11.6	-29.6	-9.3	-26.3	-9.7	-	-
Polynomial	RMSR	18.7	1.3	4.6	2.6	9.5	3.6	10.1	6.1	9.9	4.5	-	-
3^{rd} order	Rmax	-40.6	-2.4	- 9.4	6.2	-20.2	7.4	-27.3	-7.8	-23.1	-8.5	-	-

As it can be noticed in Table 2, the residuals are better for the photogrammetric method than for the polynomial methods. In the X direction, the deviation is more visible because of the elevation distortions, which are modelled in the photogrammetric method. In addition, this method allows simultaneous adjustment of all images by using common points on two or more images as tie points (coplanarity condition). This simultaneous adjustment provides better relative accuracy between the images.

In the photogrammetric method, the residuals are a good indicator of the final accuracy [8], since the correction model is one that corrects the image globally. This is not the case with the polynomial methods, which correct locally at the ground control points. It implies that distortions between the GCPs are not rigorously modelled, and consequently not entirely eliminated.

The fact that the residuals of the 3rd-order polynomial method are better than those of the 2nd order does not imply better accuracy. In the 3rd order, in fact, as there are eight additional unknowns and the same number of GCPs, the degree of freedom in the least squares adjustment is smaller, and thus reduces the adjustment residuals. Since we know the value of the 3rd-order unknowns calculated for each image, we can determine their effect on the ground or their contribution in the correction:

- for SPOT-P, we have: $3.7\ 10^{-13} \times 6{,}000^3 < 0.1$ m;
- for SAR, we have: $2.5\ 10^{-12} \times 4{,}096^2 \times 10{,}000 < 0.5$ m;
  $4.5\ 10^{-15} \times 10{,}000^3 < 0.01$ m.

These 3rd-order parameters are negligible and have no effect in the correction. Despite the results of the residuals, the 3rd-order polynomial does not allow better correction of the images. Moreover, the errors calculated on about twenty ICPs plotted on the ortho-images, are greater (10-20 m) with the 3rd-order polynomial method than with that of the 2nd order. For these reasons, the analysis of the results and the comparison of the ortho-images and their merging will not take the 3rd order into consideration.

Table 3 gives the root-mean-square errors, maximums and bias calculated on about fifty ICPs for the photogrammetric and 2nd-order polynomial methods. These ICPs, plotted on the ortho-images, are different from the 15 GCPs used in calculating the geometric correction models. These errors therefore reflect the final accuracy of the products.

TABLE 3. Root mean square, maximum and bias errors (metres) on 50 check points for the monoscopic processing.

	IMAGE	SPOT-P		SAR1-WEST		SAR2-WEST		SAR1-EAST		SAR2-EAST	
METHOD	Errors	Ex	Ey	Ex	Ey	Ex	Ey	Ex	Ey	Ex	Ey
Photogram-	RMSE	3.8	3.4	5.0	4.3	10.9	6.6	9.1	9.0	7.5	7.6
metric	Emax	- 8.7	-9.9	-11.7	8.5	-24.4	-20.2	23.7	-22.8	-17.6	15.1
	Bias	1.4	-0.1	0.2	0.0	0.3	0.3	4.1	-1.8	0.3	- 1.2
Polynomial	RMQE	30.0	16.3	13.3	10.3	21.8	14.6	15.7	10.0	21.4	9.1
2nd order	Emax	-68.1	31.8	-35.7	-25.2	-46.0	35.1	46.9	27.5	-61.8	-17.5
	Bias	-11.8	11.5	-1.8	-1.4	3.8	-2.9	3.9	-0.2	3.4	-3.3

In any case, the photogrammetric method gives better results than the polynomial method. Note that, for SPOT-P, the differences between the two methods are significantly greater, since modelling of the satellite orbit with the ephemeris is much

more accurate than modelling of the aircraft flight with only approximate values for altitude, direction and speed. As in Table 2, the differences are still greater in the X direction, primarily because of the altimetry effects, which are not corrected in the polynomial method.

The SAR-west and SAR-east mosaics and integration of the three ortho-images will therefore be achieved with an absolute error of:

- 10-15 m in the X and Y directions for the photogrammetric method; and
- 30-40 m in the X and Y directions for the polynomial method.

The qualitative evaluation of these geometric processing techniques is performed on the ortho-images and on the colour composite, which has been generated with the IHS coding. Figure 2 is a comparison of two composite subortho-images (4 by 3 km; pixel of 5 m) by the photogrammetric method (top) and by the polynomial method (bottom) to which the road vector file (accuracy of 3-5 m) has been registered. The radiometric processing performed are the same for both images.

The top image is much more homogeneous in its colours, surfaces and variations. As there is greater contrast between elements, their boundaries are clear and well defined. In the bottom image, the colour variations are greater, giving an impression of texture, and the image seems more blurred. As there is less contrast between the elements, they appear less well defined. Using the digital vector file from 1:50,000 scale topographic map, the analysis of some cartographic elements showed, in the bottom image (letters a, b and so on refer to parts of the image identified in Figure 2), that:

(a) the linear elements (roads and rivers) are either doubled or disappear (bridge, roads), due to co-registration error;
(b) the lack of sharpness in this area prevents from distinguishing the road from the forest and areas of bared soil;
(c) on surface elements, artefacts are created; there is an inversion between forest (green) and cutovers (burgundy);
(d) the texture and colour variations do not correspond to the real mapping information.

These examples, with other similar ones, clearly show that the geometric registration errors have generated radiometric merging errors, artefacts and erroneous information in the composite image. These errors do not correspond to any true information related to the ground. The road vector file, registered to these subimages, allows us to check the geometric accuracy: the visual analysis confirms the earlier statistical results for the polynomial method (30-50 m), but shows an improvement for the photogrammetric method (10 m), with maximum errors of 20 metres. These values correspond to the absolute error of registration. Validations on other areas of the image show the consistency of the results.

To confirm the quality of a rigorous geometric processing applied to various remote-sensing images, Figure 3 displays a mosaic of the eight ortho-images with the road network overlaid. The image is 39 by 29 km large with a common 10-m pixel size. From west to east, or north to south, there are the airborne SAR (C-HH), airborne CCD-MEIS sensor, SPOT-P, ERS-1-SAR (C-VV), SEASAT-SAR (L-HH), SPOT-XS (Band 2), Landsat-TM (Band 3) and MOS-MESSR (Band 2). The mosaic becomes fuzzy when viewed diagonally from the 4-m (airborne data) to the 50-m (MOS-MESSR) pixel size, resampled at 10 metres.

Figure 2: Comparison of two composite subortho-images (4 by 3 km; pixel of 5 m) by the photogrammetric method (top) and by the polynomial method (bottom), to which the road vector file (accuracy of 3-5 m) has been registered. The radiometric processing performed are the same for both images.

2.3.2. *Radiometric Processing*

As the analysis of geometric processing steps has shown that the polynomial methods affect the geometry and radiometry of the composite image, the radiometric processing steps described in 2.2 are only performed on the ortho-images geocoded by the photogrammetric method. Furthermore, only the best composite image is presented in this paper.

RGB coding is used directly by assigning SPOT-P to red, SAR-west to green and SAR-east to blue. In this combination, the characteristics of each image (SPOT-P, SAR) are well preserved. The highly visible elements on SPOT-P come out in red, and the elements oriented west and east come out in green and blue respectively. This is especially visible on river banks.

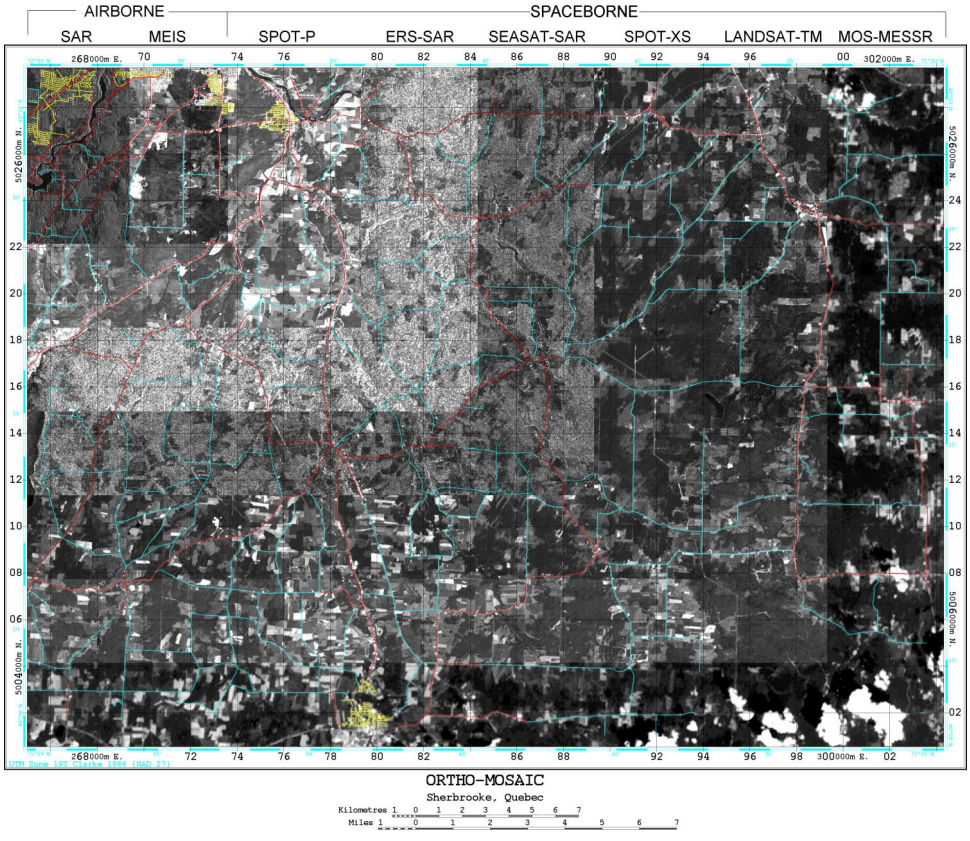

Figure 3: Mosaic of eight ortho-images (39 by 29 km10-m pixel size) with the road network overlaid. From west to east, or north to south, there are the airborne SAR (C-HH), airborne CCD-MEIS sensor, SPOT-P, ERS-1-SAR (C-VV), SEASAT-SAR (L-HH), SPOT-XS (Band 2), Landsat-TM (Band 3) and MOS-MESSR (Band 2). The mosaic becomes fuzzy when viewed diagonally from the 4-m (airborne data) to the 50-m (MOS-MESSR) pixel size, resampled at 10 metres.

The PC analysis showed that the three ortho-images were practically decorrelated and that:

- the first PC is 99% formed of SPOT-P;
- the second PC is 97% formed of SAR-west; and
- the third PC is 97% formed of SAR-east.

Thus using the three PCs contributes no more than using the three original ortho-images. Moreover, the results are often more difficult to interpret quantitatively and qualitatively because, as the statistical properties have been manipulated, the original integrity of the data has not been preserved [14].

Different IHS coding were tested and the two best one were:

- SPOT-P in I, SAR-west in H and SAR-east in S; and
- SAR-west in I, SPOT-P in H and SAR-east in S.

The first combination somewhat resembles a colour air photo since the visible SPOT-P was assigned to the intensity, which represents the brightness of colour. The highly visible elements on SPOT-P come then out very well in bright colour. As SAR-west was assigned to hue, which represents the dominant colour, it does not help provide much colour variation. Consequently, many characteristics of SAR are not visible (texture, relief and so on).

Finally, the best result is obtained with the 2nd IHS combination (Figure 4). The image has very good visual quality and effectively combines the characteristics of the various original images. It also shows much more texture because of the SAR-west assigned to intensity. The colour contrast between the forests, fields and bared soil areas is quite pronounced. This last combination seemed to be the most logical in our case, since SPOT-P covers the visible spectrum, and the higher-resolution SAR images (4 m versus 10 m), with more texture, better modulate intensity and saturation. It corresponds to tests and results of Jaskolla *et al.* [12] and Welch and Ehlers [13].

2.4. TOPOGRAPHIC MAPPING

To evaluate the mapping potential, AN image content analysis and visual interpretation of the best composite image using HIS radiometric processing (Figure 4) is performed with regards to the conventional applications of remote sensing: cartography, agriculture, forestry and geology.

2.4.1. *Cartography*

Roads can be distinguished easily because of the spatial resolution (5 m) and the contrast with other elements, such as the buildings and built-up areas. Similarly, the roads in new residential developments in forested areas are clearly visible in this image. For rivers, there is little colour variation from the SPOT-P and the moderate contrast only allows us to distinguish the boundaries. Finally, the shadows and their orientation are enhanced by the use of two SARs of opposite viewing directions; moreover, the coding of the SAR-west mosaic in intensity accentuates the texture of the image.

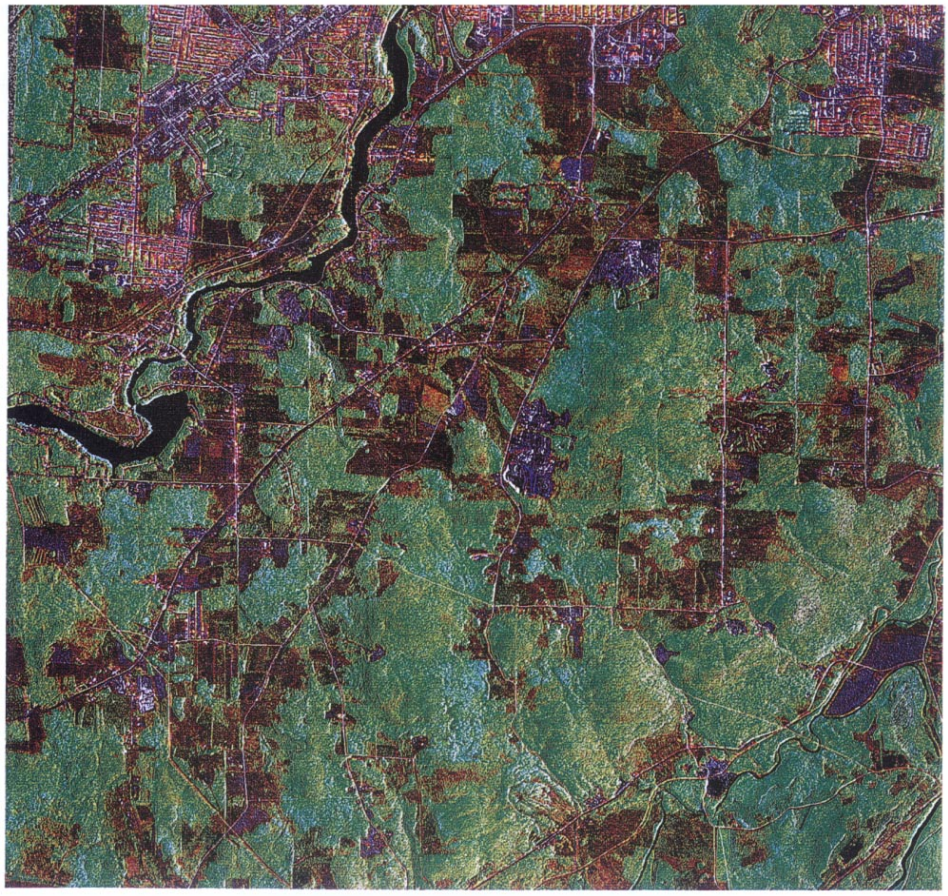

Figure 4: Composite ortho-images (10 by 10 km; 5-m pixel spacing) using IHS radiometric coding with SAR-west in I, SPOT-P in H and SAR-east in S.

2.4.2. *Agriculture*

The boundaries of fields are clearly visible. These boundaries are enhanced by fences, which are highly visible because of the prominent SAR information in these images.

For the same reason, fields containing stumps or undergoing reforestation are identifiable. As the dynamic range is great, it also allows better discrimination between land uses and between bared and cultivated fields.

2.4.3. *Forestry*
The image is very good for distinguishing forest from everything else. However, it is practically impossible to distinguish between deciduous and coniferous trees. This must come from the SPOT-P intensity image, since conifers are darker in SPOT-P images. Texture on the tree canopy related to the size of the crown and not to tree type (deciduous versus coniferous) can de discriminated. Rows of isolated trees are also visible because of their shadow. There is a visual impression of tree height superimposed on the relief, allowing us to interpret the characteristics and disturbances of stands on the basis of forest cover height. Moreover, this impression, combined with the shading, lets us distinguish rows of isolated trees.

2.4.4. *Geology*
When information on the relief is not useful, this image easily allows the distinction of more or less the same geomorphologic elements: the two NE-SW rivers and their characteristics (meanders, embankments, and bars). As soon as the interpretation requires knowledge of the relief, this composite image is much more useful due to the relief perception: stream bank slopes and glacial formations, with drumlins and ridges, which indicate the NE-SW ice advance. Similarly, NE-SW lineaments and folds, identifiable only on these two images, are probably related to the structural trend of the region.

3. Stereoscopic Processing

When no DEM is available and two images from the same sensor (VIR or SAR) are available, the stereoscopic method for feature extraction is based on traditional photogrammetric techniques. Even with two images from different sensors, the brain can generate the perception of depth, combining for example the spectral information from the Landsat-TM image and the spatial information from the SPOT-P image for the stereo plotting. The XY cartographic coordinates of the planimetric features are computed independently of its Z-altimetric coordinate, since the operator always plots in stereoscopy at the vertical of the point [15]. Consequently, the planimetric accuracy of feature positioning is not affected by any error on elevation, conversely to the previous method where any error in the DEM propagates through the geocoding process and the planimetric features.

The processing steps are more or less similar to the monoscopic method, except for the viewing parameters and the altimetry (ground control points and DEM) involved in the photogrammetric method:

- acquisition of parameters of the viewing geometry;

- acquisition of GCPs in stereoscopy: image coordinates and ground coordinates X, Y, Z;
- calculation of parameters of the stereoscopic model; and
- 3D-data extraction on the "virtual" stereo model.

Whatever the data (VIR and SAR), most of the research studies on stereoscopy around the world have focused on DEM generation [16, 17] for the topography, and very few on planimetric features extraction for cartography. Consequently, only results on DEM generation from VIR scanners and SAR sensors are presented.

3.1. VIR SCANNERS

To obtain stereoscopy with images from satellite scanners, three solutions are possible:
- the adjacent-track stereoscopy from two different orbits;
- the across-track stereoscopy from two different orbits; and
- the along-track stereoscopy from the same orbit using fore and aft images.

3.1.1. *Adjacent-track*

In the case of Landsat (MSS or TM) and Indian IRS-1A satellites, the stereoscopic acquisition is only possible from two adjacent orbits since the satellite only acquires nadir viewing images, and the tracking orbit ensures repeat path consistent within a few kilometres [18]. In fact the B/H ratio with Landsat-MSS is around 0.1, so that relief of about 4 000 m is needed to generate a parallax of five Landsat-MSS pixels (80-m resolution). Due to its quasi-polar orbit, the coverage overlap grows from about 10% at the Equator to about 85% at 80º latitude. From 50º north and south the coverage overlap (45%) enables quasi-operational experiments for elevation extraction and the accuracy of derived DEM is in the order of 50-100 m.

Consequently, the stereoscopic capabilities and applicabilities of "adjacent orbit" satellite data still remain limited because:

- it can be used for large area only in latitude higher than 45º to 50º north and south;
- it generates a small B/H ratio leading to elevation errors of more than 50 m; and
- only medium to high relief areas are suitable for generating enough vertical parallaxes.

3.1.2. *Across-track*

To obtain good geometry for a better stereo plotting, the intersection angle should be large in order to increase the stereo exaggeration factor, or equivalently the observed parallax, which is used to determine the terrain elevation. B/H ratios of 0.6 to 1.2 are typical values to meet the requirements of topographic mapping [19]. There are only few operational satellites, which have this capability to generate such B/H ratios:

- The SPOT system by steering the sensor (±26º); and

- The IRS-1C/D system by rolling the satellite (±20º).

Since the advent of the SPOT system in 1985, it is the most popular stereo capability and numerous researches around the world were performed [16]. They lead to accuracy in elevation from one to few pixels [20] depending on processing methods (photogrammetric or non-parametric), systems (intensity or feature matching) and tools (automatic, semi-automatic) used.

The new high-resolution IKONOS system, launched in September 1999, should be able to also provide across-track stereo-images, but in addition it has along-track stereo-capability by steering the sensor in any direction (±26º). If the raw data is available to end users it should confirmed the previous results achieved with SPOT data.

3.1.3. *Along-track*

In the last few years, the last solution as applied previously to space frame cameras got renewed popularity. First, the JERS-1's Optical Sensor (OPS) [21] and the German Modular Opto-Electronic Multi-Spectral Stereo Scanner (MOMS) [22] generate stereo-images by the use of forward and nadir linear array optical sensors, named OPS. The 15º forward-looking image and the nadir-looking image (18-m ground resolution) generate a stereo-pair with a B/H ratio of 0.3. The simultaneous along-track stereo-data acquisition gives a strong advantage in terms of radiometric variations versus the multi-date stereo-data acquisition with across-track stereo. This was confirmed by the very high correlation success rate (82.6%) [23]. However, the limited availability of data has restricted the evaluation of DEM generation to few research groups. They obtained accuracy for DEM of about few pixels, which are generally not as good as those obtained with across-track stereo-images.

In the next future, the Advanced Spaceborne Thermal Emission and Reflection Radiometer (ASTER) [24], the Indian IRS-P5, and most of the high-resolution satellites such as Orb-View1 and Quick-Bird and IKONOS will also be a good data source and enable better evaluations. Preliminary evaluation using aerial imagery scanned at 1-m spatial resolution showed their potential to obtain a RMS error in elevation in the range of 1.5 m to 2 m [25]. However, it is not sure that the raw imagery needed for generating DEMs and derivative topographic products will be available to the end users since, at that time, the high-resolution data resellers want to only distribute value-added products (DEM, ortho-images, mosaics).

Table 4 summarizes the general results of DEM extraction with different VIR scanners using the three stereoscopic methods. Some variations in the results occur due mainly to the different geometric modelling, image matching, editing, digital or not processing.

Table 4: Summary of the results of the elevation extraction with the VIR scanners using the stereoscopic method. The variations in the results for each stereo configuration are due to the different research studies. The values in brackets were obtained from simulated data.

Stereo-Pairs	Resolution	Adjacent-track	Across-track	Along-track
Landsat MSS	80 m	100-300 m		
Landsat TM	30 m	45-70 m		
IRS 1A	72 m	35 m		
SPOT P	10 m		5-15 m	
SPOT/Landsat	10 m/30 m		35-50 m	
IRS 1C/D	6 m		10-30 m	
MOMS-2	13.5 m			5-15 m
MOMS-2P	18 m			10-30 m
JERS OPS	20 m			20-40 m
SPOT/ERS	10 m/30 m		20-30 m	
EOS-ASTER	33 m		(15 m)	(12.5 m)
Ikonos	1 m		(1.5-2 m)	

3.2. SAR SENSORS

Due to the specific geometric and radiometric aspects of SAR images, it may take our brain time to perceive the terrain relief with SAR stereo-images, mainly when both geometric and radiometric disparities are large [26]. However, since depth perception is an active process (brain and eye) and relies on an intimate relationship with object recognition, radar images can be viewed in stereo as easily as VIR satellite images after training. Stereo parallaxes predominate when viewing radar images, but the shade and shadow cues also have a strong and cumulative effect. For example, with a quasi-flat terrain, the shade and shadow cues overcome the stereo effect when viewing pseudoscopically a radar stereopair [27].

To obtain good geometry for stereoplotting, the intersection angle (Figure 5) should be large in order to increase the stereo exaggeration factor, or equivalently the observed parallax, which is used to determine the terrain elevation. Conversely, to have good stereo-viewing, the interpreters (or the image matching software) prefer images as nearly identical as possible, implying a small intersection angle. Consequently, large geometric and radiometric disparities together hinder stereo-viewing and precise stereoplotting. Thus, a compromise has to be reached between a better stereo-viewing (small radiometric differences) and more accurate elevation determination (large parallax).

The common compromise for any type of relief is to use a same-side stereopair, thus fulfilling both conditions above. It was realized with SIR-B [28], SIR-C [29], ERS [30] and JERS [23]. Unfortunately, this does not maximise the full potential of stereo radar for terrain relief extraction. Another potential compromise is to use opposite-side stereopairs over rolling topography [15]. The rolling topography reduces the parallax difference and also the radiometric disparities (no layover and shadow, little foreshortening) making possible simultaneously good stereo-viewing and accurate stereoplotting. A last approach to minimise the geometric disparities is to pre-process

the images using a large grid spacing or low accuracy DEM, as it has been applied with success to iterative hierarchical SAR image matching [28].

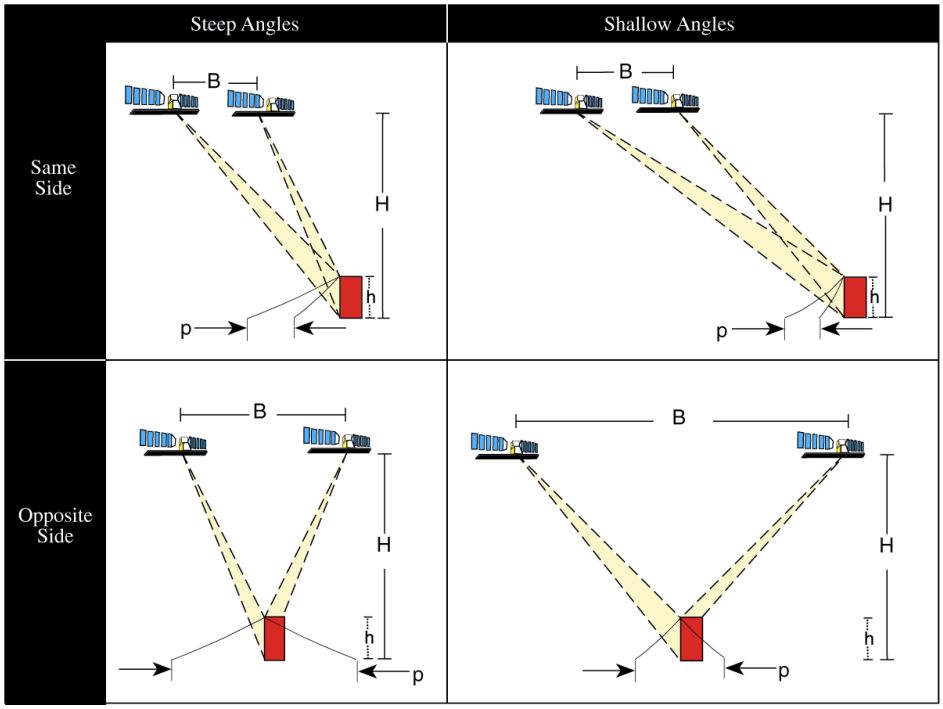

Figure 5: The intersection geometry with the radar parallax (p) due to the terrain elevation (h) for different stereo SAR configurations (same-side versus opposite-side; steep versus shallow look-angles).

Since the last ten years, most of the results on DEM generation with SAR stereo-images have been inconsistent and practical experiments do not clearly support theoretical expectations [31]. For example, larger ray intersection angles and higher spatial resolution do not translate into higher accuracy. In various experiments, accuracy trends even reverse, especially for rough topography. Only in the extreme case of low relief, does accuracy approach the theoretical expectations. The main reason is that the error modelling accounts only for SAR geometric aspects (look and intersection angles, range error) and completely neglects the radiometric aspects (SAR backscatter) of the stereopair and of the terrain.

Since SAR backscatting, and consequently the image radiometry, is much more sensitive to the incidence angle that the VIR reflectance, especially at low incidence angles, the possibility of using theoretical error propagation as a tool for predicting accuracy and selecting appropriate stereo-images for DEM generation is very limited. Therefore, care must be taken in attempting to extrapolate VIR stereo concepts to SAR.

Previously to RADARSAT, Canada's first earth observation satellite launched in November 1995, it was difficult to acquire different stereo configurations to address the above points. RADARSAT with its various operating modes, imagery from a broad range of look directions, beam positions and modes at different resolutions [32] fills this gap. Under the Applications Development and Research Opportunity (ADRO) program sponsored by the Canadian Space Agency, researchers around the world have undertaken studies on the stereoscopic capabilities by varying the geometric parameters (look and intersection angles, resolution, etc.). Most of the results were presented at the final RADARSAT ADRO Symposium "Bringing Radar Application Down to Earth" held in Montreal, Canada in 1998 [17]. There was a general consensus on the achieved DEM extraction accuracy: a little more (12 m) and a little less (20 m) than the image resolution for the fine mode and the standard mode respectively, whatever the method used (digital stereoplotter or image matching). Relative elevation extraction from a fine mode RADARSAT stereopair for the measurement of canopy heights in the tropical forest of Brazil was also addressed [27].

However, there were no significant correlations between the DEM accuracy and the intersection angle in the various ADRO experiment results. This confirmed the same contradiction found with SIR-B [29]. In fact, most of the experiments showed that the principal parameter that has a significant impact on the accuracy of the DEM is the type of the relief and its slope. The greater the difference between two look-angles (large intersection angle), the more the quality of the stereoscopic fusion deteriorated. This cancels out the advantage obtained from the stronger stereo geometry, and is more pronounced with high-relief terrain. On the other hand, although a higher resolution (fine mode) produced a better quality image, it does not change the stereo acuity for a given configuration (e.g. intersection angle), and it does not improve significantly the DEM accuracy. Furthermore, although the speckle creates some confusion in stereoplotting, it does not degrade the DEM accuracy because the matching methods or the human stereo-viewing "behave like a filter". Preprocessing the images with an adaptive speckle filtering does not improve the DEM accuracy with a multi-scale matching method [30]; it can slightly reduce the image contrast and smoothes the relief, especially the low one [26].

Since the type of relief is an important parameter influencing the DEM accuracy, it is strongly recommended that the DEM accuracy be estimated for different relief types. Furthermore, in the choice of a stereoscopic pair for DEM generation, both the geometric and radiometric characteristics must be jointly evaluated taking into account the SAR and surface interaction (surface geometry, vegetation, soil properties, geographic conditions, etc.). The advantages of one characteristic must be weighted against the deficits of the other. Table 5 summarizes the general results of DEM extraction with SAR scanners using the stereoscopic method.

TABLE 5. Summary of the results of the elevation extraction with the SAR sensors using the stereoscopic method. The variations in the results for each stereo configuration are due to the different research studies.

Satellite	SAR Band-Polarisation	Resolution (m)	Relief	Accuracy (m)	
				Same-Side	Opposite-Side
SIR A	L-HH	25	High	100	
SIR B	L-HH	40	Medium	25	
			High	60	36
ERS 1/2	C-VV	24	Medium	20	20
			High	45	
JERS	L-VV	18	High	75	
Almaz	S-HH	15	High	30-50	
RADARSAT	C-HH	F[a] 7-9	Low	8-10	20
		S[a] 20-29	Medium	15-20	40
		W[a] 20-40	High	25-30	

4. Conclusion

Two conventional methods (monoscopic and stereoscopic) to process remote sensing images for extracting 2D or 3D information have been presented.

The monoscopic method requires rigorous geometric and radiometric processings. The superiority of the rigorous geometric processing is mainly due to the fact that the mathematical model corresponds to the physical reality of the viewing geometry and takes into account the distortions caused by relief. This superiority will also increase with mountainous terrain. This rigorous geometric processing will facilitatd subsequent processing operations, while the polynomial geometric processing will require more complicated processing operations to remove the artefacts and false information. Furthemore, because the latter do not correspond to any physical reality and depend on viewing conditions (images, ground and so on), the subsequent processing techniques are dependent on the specific viewing conditions, and will not apply with another set of images under different viewing conditions. It thus limits the use and future applications of such image processing techniques.

Consequently, the monoscopic processing of multisource data requires rigorous geometric correction to obtain a subpixel accuracy, as well as appropriate radiometric processing, which take into account the nature and characteristics of the data. It then ensures that the composite image preserves the best of the information from each image and maintains data integrity.

On the other hand, the stereo capability of different satellites with different methods has been addressed: adjacent-orbit stereo with Landsat and IRS-1A, across-track stereo with SPOT and IRS-1C, along-track stereo with JERS and MOMS, same and opposite-stereo with ERS and RADARSAT.

Since any sensor, system or method has its own advantages and disadvantages, future solution for operational DEM generation should use the complementarity between the different sensors, systems, methods and processing. Furthermore, it has been proven in most of the previous experiments that the user has to make judgements and decisions at different stages of the processing, regardless of the level of automatic processing to obtain the final DEM product. Non-exhaustive examples of complementarity are listed below:

- to use mixed-sensor (VIR and SAR) stereoscopic images in order to obtain the second image of the stereo-pair in cloud-cover area;
- to combine VIR and SAR stereoscopic images where the radiometric content of the VIR image is combined with the SAR high sensitivity to the terrain relief and its "all-weather" capability;
- to use the visual matching to seed points to the automatic matching or to post-process and edit raw DEMs (occlusion, shadow or mismatch areas);
- to use stereo measurements of objects edges and other geomorphological features (thalweg and crest lines, break lines, lake boundary and elevation) to increase the consistency of the DEM;
- to combine the "know-how" of the users with the computer capability.

5. Acknowledgements

The author would like to thank NATO and CCRS in their support. Ms. Liyuan Wu and Mr. René Chenier of Consultants TGIS inc., who performed image processing, are also acknowledged.

6. References

1. Guertin, F. and Shaw, E. (1981) Definition and potential of geocoded satellite imagery products, *Proceedings of the 7th Canadian Symposium on Remote Sensing*, held in Winnipeg, Canada, September 8-11, Manitoba Remote Sensing Centre, Canada, 384-394

2. Clark, J. (1980) Training site statistics from Landsat and Seasat satellite imagery registered to a common map base, *Proceedings of the ASPRS Semi-Annual Convention*, Niagara Falls, U.S.A., American Society of Photogrammetry, RS.1.F.1-RS.1.F.9

3. Murphrey, S.W. (1978) SAR-Landsat image registration study, Final report, IBM Corp., Gaithersburg, MD, USA.

4. Anuta, P.E., Freeman, D.M., Shelly, B.M. and Smith, C.R. (1978) SAR-Landsat image registration systems study, LARS Contract Report 082478, Purdue University, Ind., U.S.A.

5. Daily, M., Farr, T., Elachi, C. and Schuber, G. (1979) Geologic interpretation from composite radar and Landsat imagery, *Photogrammetric Engineering and Remote Sensing*, **45**, 1109-1116.

6. Guindon, B., Harris, J.W.E., Teillet, P.M., Goodenough, D.G. and Meunier, J.F. (1980) Integration of MSS and SAR data for forested regions in mountainous terrain, *Proceedings of the 14th International Symposium of Remote Sensing Engineering* held in San Jose, Costa Rica, ERIM, USA, 79-84.

7. Zobrist, A.L., Blackwell, R.J. and Stromberg, W.D. (1979) Integration of Landsat, Seasat and other geodata sources, *Proceedings of the 13th Annual Symposium on Remote Sensing of the Environment*, ERIM, Ann Arbor, USA, 271-279.

8. Toutin, Th. (1995) Multi-source Data Fusion with an Integrated and Unified Geometric Modelling, *EARSeL Journal Advances in Remote Sensing*, **4**, 118-129.

9. Livingstone, C.E., Gray, A.L., Hawkins, R.K., Olsen, R.B., Halbertsma, J.G. and Deane, R.A. (1987) CCRS C-band airborne radar: system description and test results, *Proceedings of the 11th Canadian Symposium on Remote Sensing*, Waterloo, Canada, 22-25 June, University of Waterloo, Canada, 379-395.

10. Colwell, R.N. (1983) *Manual of Remote Sensing*, 2nd edition, Vol. 1, Sheridan Press, Falls Church, Virginia, U.S.A.

11. Chavez, P.S. Jr., Sides, S.C., and Anderson, J.A. (1991) Comparison of three different methods to merge multiresolution and multispectral data: Landsat-TM and SPOT panchromatic, *Photogrammetric Engineering and Remote Sensing*, **57**, 295-303.

12. Jaskolla, F., Rast, M., and Bodechtel, J. (1985) The use of SAR system for geological applications, *Proceedings of the Workshop on Thematic Applications of SAR Data*, Frascati, Italy, SP-257, ESA, Paris, 41-50.

13. Welch, R. and Ehlers, M. (1988) Cartographic feature extraction with integrated SIR-B and Landsat-TM images, *International Journal of Remote Sensing*, **9**, 873-889.

14. Harris, J.R., Murray, R. and Hirose, T. (1990) IHS transform for the integration of radar imagery with other remotely sensed data, *Photogrammetric Engineering of Remote Sensing*, **56**, 1631-1641.

15. Toutin, Th. (1996) Opposite-side ERS-1 SAR stereo mapping over rolling topography, *IEEE Transactions on Geoscience and Remote Sensing* **34**, 543-549.

16. Centre National d'Études Spatiales (CNES) (1987) *SPOT-1 : Utilisation des images, bilan, résultats, Proceedings of the SPOT-1 Symposium*, Paris, France, CNES, Toulouse, France.

17. Canadian Space Agency (CSA), 1998, "Bringing Radar Application Down to Earth", *Proceedings of the RADARSAT ADRO Symposium*, Montreal, Canada, October 13-15, CD-ROM.

18. Simard, R., 1983, "Digital stereo-enhancement of Landsat-MSS data", *Proceedings of the Seventeenth International Symposium on Remote Sensing of Environment*, ERIM, Ann Arbor, MI, USA, May 9-13, 1275-1281.

19. Light, D.L., Brown D., Colvocoresses A., Doyle F., Davies M., Ellasal A., Junkins J., Manent J., McKenney A., Undrejka R. and Wood G. (1980) Satellite photogrammetry, Chapter XVII in *Manual of Photogrammetry*, ASPRS, Bethesda, USA, pp. 883-977.

20. Toutin, Th. (1995) Generating DEM from stereo images with a photogrammetric approach: Examples with VIR and SAR data, *EARSeL Journal Advances in Remote Sensing*, **4**, 110-117.

21. Maruyama, H., Kojiroi R., Ohtsuka T., Shimoyama Y., Hara S. and Masaharu H. (1994) Three dimensional measurement by JERS-1, OPS stereo data, *International Archives for Photogrammetry and Remote Sensing*, Athens, Ga, USA, **30**, 210-215.

22. Ackerman, F., Fritsch D., Hahn M., Schneider F. and Tsingas V. (1995) Automatic generation of digital terrain models with MOMS-02/D2 data, *Proceedings of the MOMS-02 Symposium*, Köln, Germany, July 5-7, EARSeL, Paris, France, 79-86.

23. Raggam, J. and Almer A. (1996) Assessment of the potential of JERS-1 for relief mapping Using optical and SAR data, *International Archives of Photogrammetry and Remote Sensing*, Vienna, Austria, July 9-18, Austrian Society for Surveying and Geoinformation, Vienna, Austria, **31**, B4, 671-676.

24. Tokunaga, M., Hara S., Miyazaki Y. and Kaku M. (1996) Overview of DEM product generated by using ASTER data, *International Archives of Photogrammetry and Remote Sensing*, Vienna, Austria, July 9-18, Austrian Society for Surveying and Geoinformation, Vienna, Austria, **31**, B4, 874-878.

25. Ridley, H.M., Atkinson P.M., Aplin P., Muller J.-P. and Dowman I. (1997) Evaluation of the potential of the forthcoming US high-resolution satellite sensor imagery at the ordnance survey, *Photogrammetric Engineering and Remote Sensing*, **63**, 997-1005.

26. Toutin, Th. (1999) Error tracking of radargrammetric DEM from RADARSAT images. *IEEE Transactions on Geoscience and Remote Sensing,* **37**, 2227-2238.

27. Toutin, Th. and Amaral S. (2000) Stereo RADARSAT data for canopy height in Brazilian forest. *Canadian Journal for Remote Sensing* **26,** (in press).

28. Simard, R., Plourde F. and Toutin Th. (1986) Digital elevation modelling with stereo SIR-B image data. *International Archives of Photogrammetry and Remote Sensing,* **26**, 161-166.

29. Leberl, F., Domik G., Raggam J., Cimino J., and Kobrick M. (1986) Multiple incidence angle SIR-B experiment over Argentina: stereo-radargrammetric analysis. *IEEE Transactions on Geoscience and Remote Sensing* **24**, 482-491.

30. Dowman, I.J., Twu Z.-G., Chen P.H. (1997) DEM generation from stereoscopic SAR data. Proceedings *ISPRS Joint Workshop on Sensors and Mapping from Space*, Hannover, Germany, September 29-October 2, 113-122.

31. Leberl, F. (1990) *Radargrammetric image processing*. Artech House, Norwood, USA.

32. Parashar, S., Langham E., McNally J., Ahmed S. (1993) RADARSAT mission requirements and concepts, *Canadian Journal of Remote Sensing* **18**, 280-288.